Hindawi
International Journal of Aerospace Engineering
Volume 2022, Article ID 2164485, 13 pages
https://doi.org/10.1155/2022/2164485

Research Article

Thermal-Structural Analysis of the Support Structure for a Modular Space Deployable Antenna

Lu Jin,[1] **Feiyang Zhang**,[1] **Dake Tian**,[2] **Qinghe Wang**,[1] **and Quanyu Cao**[1]

[1]*School of Civil Engineering, Shenyang Jianzhu University, Shenyang 110168, China*
[2]*School of Mechanical Engineering, Shenyang Jianzhu University, Shenyang 110168, China*

Correspondence should be addressed to Dake Tian; tiandake@sjzu.edu.cn

Received 10 February 2022; Revised 18 April 2022; Accepted 21 April 2022; Published 3 June 2022

Academic Editor: Tuanjie Li

Copyright © 2022 Lu Jin et al. This is an open access article distributed under the Creative Commons Attribution License, which permits unrestricted use, distribution, and reproduction in any medium, provided the original work is properly cited.

A modular space deployable antenna has the advantages of extensibility, adaptability, and versatility, which is an ideal structure to meet the development trend of large aperture, high precision, and light weight for the deployable antenna in the future. To date, there are few reports on the temperature response of a modular deployable antenna in the thermal alternating environment in orbit. The aim of this study is at investigating the influence of a modular deployable antenna support structure on the surface accuracy and stability under the space thermal alternating environment. For this purpose, the thermal-structure analysis of the deployable antenna support structure was carried out by ANSYS APDL finite-element software. Using the transient temperature field obtained by thermal analysis as the boundary condition, the coupling law of stress development and thermal deformation of the support chord and cable caused by the antenna structure constraint position and other parameters is analyzed. In a uniform thermal field, the thermal stress of cables in the central module of the structure is the highest and that of the chord components in the same-circle modules is essentially the same. The thermally stress of the upper chords increases progressively toward the outer module, whereas that of cables decreases in the same direction. The thermal deformation at the upper-layer centroid of the structure can reach about 15 mm, so the influence on the accuracy of the antenna cannot be ignored. When the splicing vertical rod of adjacent modules in the outermost of the support structure is taken as the constraint connecting with the extension arm, the thermal deformation of the structure is minimum. The heat-insulating composite coating should be adopted on the surface of the antenna structure to reduce the thermal deformation and improve the adaptability. The thermal-structural analysis model proposed in this study could accurately estimate the behaviour of thermal deformation for the modular space deployable antenna, but the further coupling condition of the nonuniform temperature field could still be conducted. The results can provide a reference for the basic theory and engineering application of thermal-structural analysis for extralarge-aperture modular deployable antennas in the future.

1. Introduction

The deployable antenna plays an important role in the transmission and acquisition of information in the aerospace and defence fields. This new type of space deployable structure is the product of the rapid development of aerospace science and technology over the past two to three decades [1, 2]. Deployable antennas have already been widely applied in various fields, including space communications, military reconnaissance, earth observation, and satellite navigation [3–6]. Given the increasing demand for a precise satellite service in deep space exploration, the thermal response of the deployable antenna support structure to the harsh space environment has become important considerably. As a satellite moves in an orbit, the support structure of a deployable antenna is subject to thermodynamic issues induced by solar radiation, such as vibration and the resulting stress and deformation [7–9]. Especially for large-aperture modular deployable antenna, these problems occur most commonly when the antenna passes through the Earth's shadow.

Thermally induced vibrations were first theoretically predicted by Boley [10], who also established a basis for vibration parameter determination. In the decades that followed, the subject of thermally induced structural response attracted

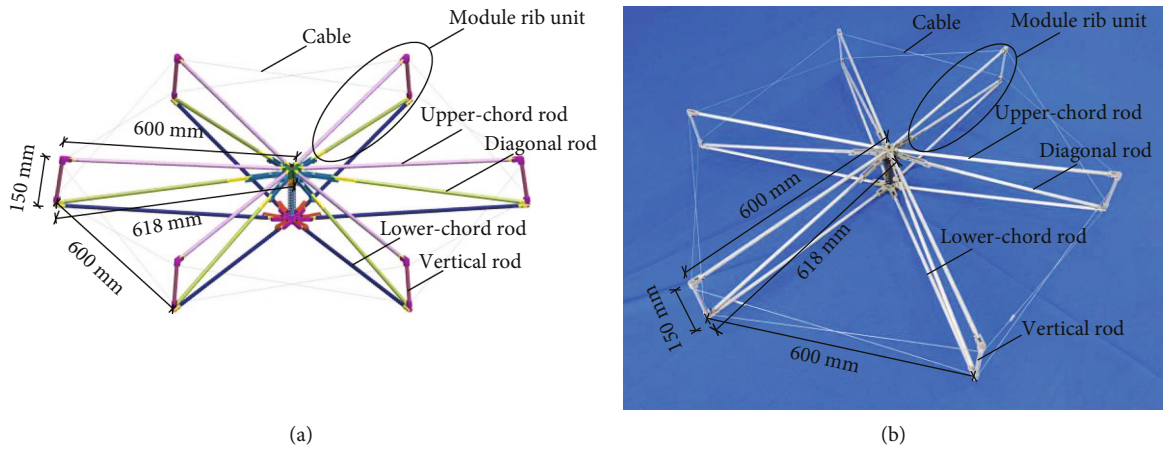

Figure 1: A single module. (a) The three-dimensional prototype. (b) The single-module prototype.

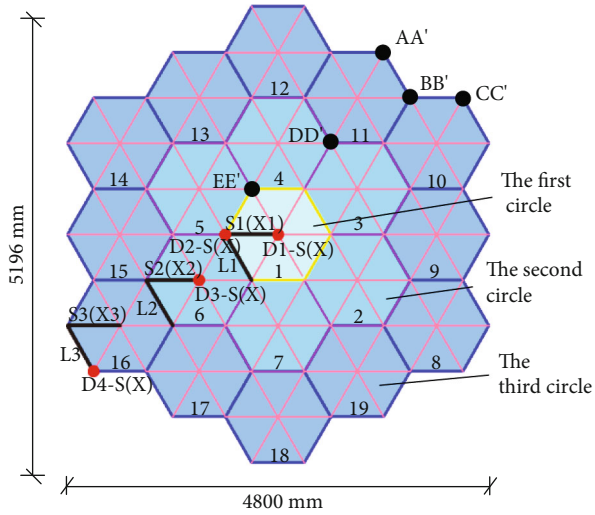

Figure 2: Module arrangement with the marked points and rods.

attention from scholars and researchers worldwide. For example, by analyzing bending vibrations of the Hubble Space Telescope solar arrays, Thornton and Kim [11] determined the coupling between the dynamic response of the structure and transient temperature field and the basis is established for determining the stability of bending vibrations. Namburu and Tamma [12] reported that there are significant differences between the dynamic response of deployable members under the action of general linear thermal effects and those under nonlinear thermal effects. Johnston and Thornton [13] examined spacecraft attitude disturbances resulting from thermally induced deformations of flexible appendages and determined that the attitude response of the system is related to the ratio of the thermal and structural response times of flexible appendages. Zhang [14] conducted temperature field analysis, thermal stress analysis, and structural deformation simulation analysis for a deployable parabolic antenna with a 5 m diameter. Ding and Xue [15] used the Fourier-finite-element method to simulate the thermal response of aerospace structures with thin-walled tubular components in the transient temperature field and thereby provided an effective method for analyzing the transient temperature field and thermal deformation of the complex aerospace structure. Rodriguez et al. [16] developed the thermocryogenic technology for the thermocryogenic system of the tropospheric emission spectrometer, and this in turn maximised the overall performance of the instrument. Fan et al. [17] studied the thermal-dynamic coupling of the in-orbit structure with flexible appendages using a modified Lagrange-finite-element method. Liu et al. [18] conducted a study on thermally induced vibrations of a deployable rib antenna using the finite-element method and showed that thermal vibrations affect the surface accuracy of the antenna structure. Abbas et al. [19] developed a three-dimensional rectangular plate element with variable thicknesses for panels of re-entry vehicles, which is exposed to a severe thermal environment under a supersonic flow condition. Sun [20] simulated and analyzed the structural strength and dynamic properties of a deployable spiral antenna in the extreme thermal environment of space and thereby provided a guiding reference for the antenna structure design. Yun and Yuan [21] conducted thermal-structural analysis of a deployable hoop antenna, and it is demonstrated that when passing through the Earth's shadow in orbit, the antenna structure is subjected to significant overall structural deformation in a nonuniform temperature field. Wu et al. [22] conducted thermal-structural analysis of a deployable hoop antenna and determined that the temperature field significantly impacts an antenna's surface tension and shape accuracy. In summary, the thermal-structural coupling response of large-aperture space deployable antenna structures cannot be neglected because it considerably impacts the vibration and deformation of the antenna surface [23, 24].

Furthermore, large aperture, high precision, and light weight have become the trend of antenna development. The modular space deployable antenna studied in this paper is a new kind of space structure with great development potential and value, which meets the development trend of large aperture and high precision of the antenna. Based on the topological theory, the modular element can meet the development trend and requirements of 100-meter aperture of the antenna in the future. For the extralarge-aperture antenna, dense rods and shadow occlusion of extralarge-aperture mesh are

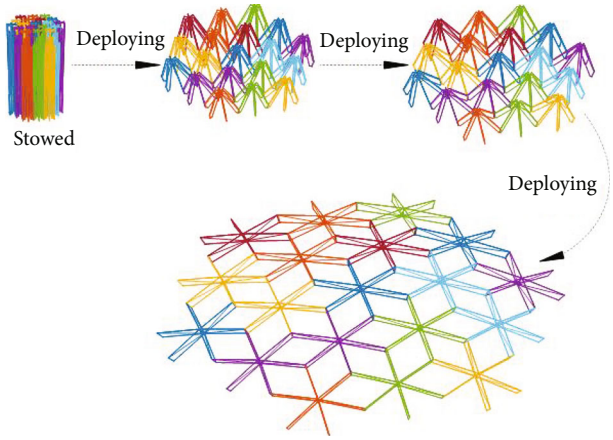

Figure 3: The deployment process of 3-circle 19-module antenna support structure (without cables).

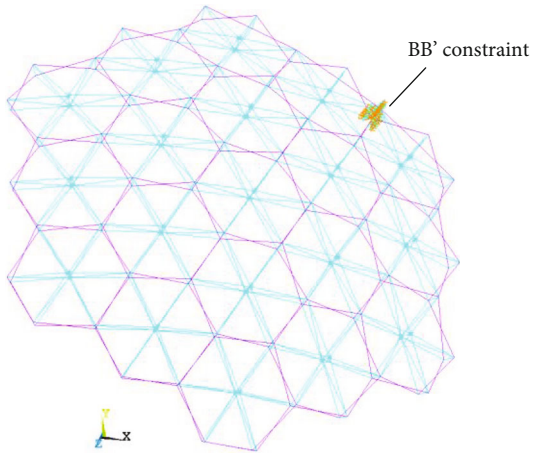

Figure 4: FEM of the modular deployable antenna.

Table 1: Thermophysical parameters of antenna materials.

Material property	Aluminum alloy	Steel cable
Elastic modulus: E (GPa)	70	150
Poisson ratio: μ	0.31	0.3
Density: ρ (kg/m^3)	2840	7850
Thermal conductivity: k (W/m/K)	195	49.8
Specific heat capacity: c (J/kg)	924	465
Thermal expansion coefficient: α (K^{-1})	2.2×10^{-5}	1.2×10^{-5}
Emissivity: ε	0.6	0.26
Radiation absorptivity: ε_1	0.9	0.9

obvious. The thermal-induced deformation and thermal-induced vibration pose more significant threat to the performance of the antenna in orbit. It will also restrict its future application. However, there is a paucity of analytical studies in this area and only fewer cases have been applied in orbit.

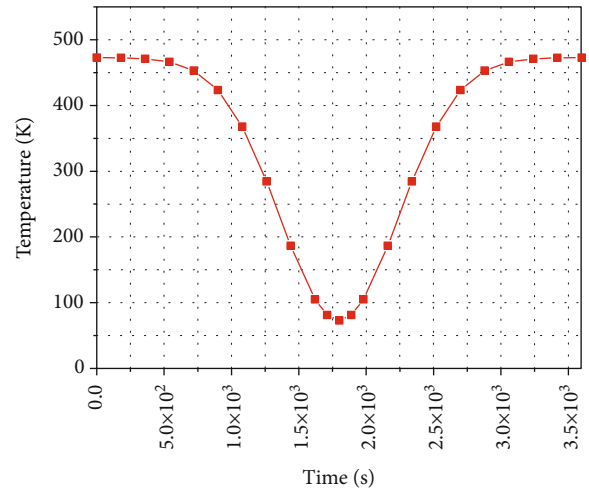

Figure 5: Temperature distribution of the transient temperature field.

In this study, thermal-structural analysis of a modular space deployable antenna in the transient thermal field is analyzed, whose basic configuration is composed of 19 hexagonal modules with a diameter of 5 meters. Furthermore, the thermally induced stress of different rod and cable elements of the support structure and the deformation of the key points include the centroid point and the farthest point away from structural constraint is considered. The trends of thermally induced overall deformation are compared for different constraint positions of the antenna structure to provide a basis for selecting the safest and most optimal design for the support structure for the modular space deployable antenna. In addition, the research results can provide a reference for the basic theory and engineering application of thermal-structural analysis for extralarge-aperture modular deployable antennas in the future.

2. Finite-Element Model and Validation

2.1. Structure of the Modular Deployable Antenna. The antenna structure is a support back frame after the deployment and locking of the space deployable antenna, which is composed of a plurality of hexagonal modules arranged topologically according to the accuracy of the antenna network [25, 26]. Firstly, a rib unit is composed of upper chord and lower chord rods, a diagonal web rod, and a vertical rod and the length of the upper and lower chord rods is 600 mm, the length of the diagonal web rod is 618 mm, and the length of the vertical rod is 150 mm; then, a single-hexagon module with a side length of 600 mm is composed of six rib units and a cable (Figure 1). Figure 1(a) is the three-dimensional prototype of a single module, and Figure 1(b) is the single-module prototype.

The single-module topology forms a 3-circle 19-module antenna structure with a size of 4800 mm × 5196 mm (Figure 2). The topological positions, number of circles, and marking points of each module are shown in Figure 2.

Table 2: Statistical analysis of thermal stress and deformations.

Time (s)	Maximum deformation (mm)	Deformation at the upper centroid (mm)	Maximum stress of chord rod (MPa)	Maximum stress of cable (MPa)	Maximum stress of constraint (MPa)
1	32.05	13.15	50.67	47.94	3.94
180	32.00	13.12	50.56	47.83	3.93
360	31.75	13.02	50.17	47.46	3.9
540	30.90	12.66	48.81	46.18	3.8
720	28.54	11.71	45.12	42.7	3.51
900	23.25	9.53	36.76	34.79	2.85
1080	13.37	5.48	21.13	20.01	1.63
1260	−1.51	−0.62	−2.38	−2.26	−0.18
1440	−18.97	−7.74	−29.94	−28.42	−2.30
1620	−33.02	−13.45	−52.90	−50.30	−4.05
1710	−37.44	−15.26	−59.53	−56.54	−4.56
1800	−39.02	−15.91	−61.92	−58.84	−4.72
1915	−37.44	−14.77	−59.53	−56.54	−4.56
1980	−33.02	−13.45	−52.90	−50.30	−4.05
2160	−18.97	−7.74	−29.94	−28.42	−2.30
2340	−1.51	−0.62	−2.38	−226	−0.18
2520	13.37	5.48	21.13	20.01	1.63
2700	23.25	9.53	36.76	34.79	2.85
2880	28.54	11.71	45.12	42.7	3.51
3060	30.90	12.66	48.81	46.18	3.8
3240	31.75	13.02	50.17	47.46	3.9
3420	32.00	13.12	50.56	47.83	3.93
3600	32.05	13.15	50.67	47.94	3.94

As shown in Figure 2, there is 1 module in the first circle and there are 6 and 12 modules in the second and third circles, respectively. AA′, BB′, CC′, DD′, and EE′ represent the position of splicing vertical rods, S1 represents the no. 1 upper chord, X1 represents the no. 1 lower chord, L1 represents the no. 1 cable, and D1-S and D1-X represent the no. 1 point of the upper layer and lower layer, respectively.

Figure 3 shows the expansion process of a 3-circle 19-module support structure from a folded state to a deployed state. After expansion, its total size is 4800 mm × 5196 mm, in which the upper chord forms an inner concave surface and the lower chord forms an outer convex surface. The model is based on the principle prototype in the previous work. The geometry size of the antenna structure is 1 : 1 restored, and the appearance design of the deployable antenna is basically consistent with the actual structure. The main structure of the principle prototype is made of aluminum alloy, and the theoretical and experimental research on the unfolding function, unfolding characteristics, unfolding accuracy, and dynamics characteristics has been completed. In the model of Figure 3, all rod members of the structure are 2A12 aluminum alloy hollow round rods, the vertical rod outer diameter is 12 mm, and the inner diameter is 10 mm. The outer diameter of the upper and lower chords and inclined rods is 10 mm and the inner diameter is 8 mm. The cable is a steel wire cable whose diameter is 1 mm.

2.2. Model Establishment. APDL was used to build the finite-element model of the modular deployable antenna as shown in Figure 4. In the thermal stress analysis, the displacement and rotation angles of the vertical rod BB′ connecting two outermost modules are constrained because this component is connected to the deployment arm of the satellite antenna. After deployment, the overall stability of the support structure is maintained via tension cables and rigidly connected rods; the cable applied 200 N preload. The thermophysical parameters of the antenna materials are shown in Table 1.

3. Transient Thermal Analysis

3.1. Theoretical Basis of Temperature Field Analysis. The temperature field is closely related to the geometry of the structure. Based on the principle of heat transfer theory, the governing differential equation of heat conduction of the three-dimensional object can be written as [27]

$$\frac{\partial}{\partial x}\left(k_x \frac{\partial T}{\partial x}\right) + \frac{\partial}{\partial y}\left(k_y \frac{\partial T}{\partial y}\right) + \frac{\partial}{\partial z}\left(k_z \frac{\partial T}{\partial z}\right) = \rho c \frac{\partial T}{\partial t}, \quad (1)$$

where k_x, k_y, and k_z are the coefficients of thermal conductivity of rod elements in x, y, and z directions in space; ρ denotes the density of the material; c denotes the specific heat capacity of the material.

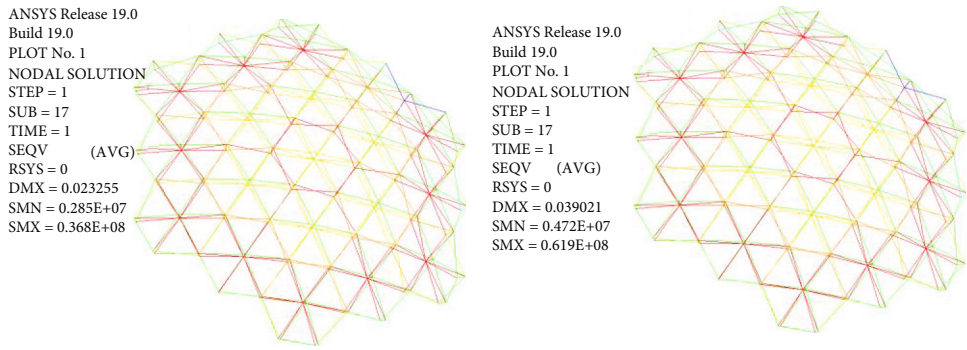

(a) (b)

Figure 6: Thermal stress distribution. (a) $t_1 = 900$ s. (b) $t_2 = 1800$ s.

The radiation boundary condition is assumed as follows:

$$-\left(k_x \frac{\partial T}{\partial x} n_x + k_y \frac{\partial T}{\partial y} n_y + k_z \frac{\partial T}{\partial z} n_z\right) = aXT^4 - Tq_r.. \quad (2)$$

The initial condition is as follows:

$$T(x, y, z)_{t=0} = T_0, \quad (3)$$

where n_x, n_y, and n_z are the direction cosines of the outer normal of rod elements in three directions, a denotes the Stefan Boltzmann constant ($5.67 \times 10^{-8}\text{W/m}^2/\text{K}^4$), X denotes the coefficient of blackness, T denotes the structure of temperature, q_r denotes the radiant heat flow density per unit area, and T_0 denotes the initial temperature of structure.

According to the Galerkin method, it can be deduced in formulas (1)–(3) as follows:

$$[C]^e \frac{\partial}{\partial t}\{T(t)\}^e + ([K_k]^e + [K_r]^e)\{T(t)\}^e = \{F_r\}^e, \quad (4)$$

where $[C]^e$ denotes the heat capacity matrix of the structural element, $[K_k]^e$ denotes the heat transfer matrix of the structural element, $[K_r]^e$ denotes the thermal radiation matrix of the structural element, and $\{F_r\}^e$ denotes the thermal load vector of the structural element.

Then, the temperature field calculation equation of the structure at t moment can be obtained:

$$\left(\frac{[C]}{\Delta t} + [K_k + K_r]\right)\{T(t)\}_t = \{F_r\} + \frac{[C]}{\Delta t}\{T(t)\}_{t-\Delta t}, \quad (5)$$

where Δt denotes the time step.

Basing on the abovementioned temperature field solution and the working environment in orbit, the calculation of the thermal analysis model of the antenna structure is simplified and assumed, so that the thermal analysis and the thermal-structural coupling analysis are more suitable for the practical engineering application of the antenna in orbit.

To simplify the thermal-structural analysis, the following basic assumptions are adopted:

(a) The antenna enters and leaves the Earth's shadow area for 1 h, i.e., 3600 s

(b) The temperature change of the antenna structure in the radiant during 3600 s is within the range 73.15 K~473.15 K

(c) The effect of shadow occlusion is not considered so that each element of the antenna support structure receives the same amount of radiation in each period

The fit curve of the temperature change during the time when the antenna moves in and out the Earth's shadow is used to obtain the temperature change function as follows:

$$T(t) = T_0 - T_S \times e^{-0.5\times((t-t_c)/\tau)^2}, \quad (6)$$

where T_S denotes the magnitude of temperature change, t_c denotes the experience time of entering the shadow area fully, $t_c = 1800$ s, τ denotes the characteristic time for thermal response, and $\tau = 440.2$ s [28].

3.2. Thermal Analysis. Based on the aforementioned assumptions, in the thermal analysis of the antenna structure using APDL, LINK33 is used to simulate the temperature element of chord rods and cables and MASS71 is used to simulate concentrated mass components. Figure 5 shows the temperature distribution curve of the deployable antenna obtained using the FEM simulation in the transient temperature field. When the metal mesh surface of the antenna is not considered, the shadow occlusion effect is not obvious. Therefore, the shadow occlusion is not considered in the thermal analysis for the support structure in this paper and the temperature field distribution of the whole antenna structure is uniform at each moment and the temperature of each rod of the whole antenna structure is the same. For example, at $t_1 = 900$ s and $t_2 = 1800$, the overall temperatures of the structure are 423.517 K and 73.168 K, respectively.

It can be seen in Figure 5 that the temperature decreases slowly when the antenna begins to pass through the Earth's

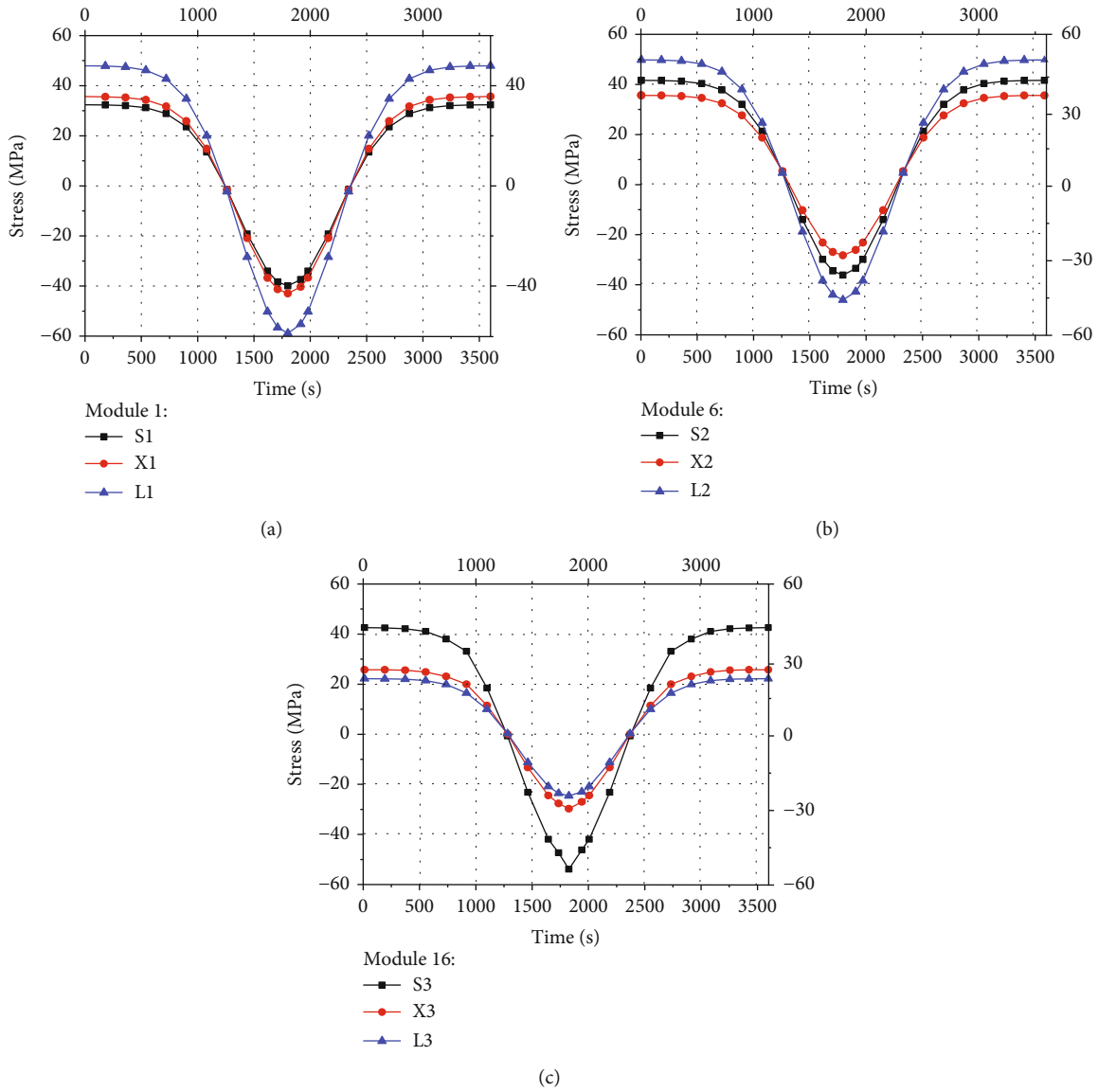

Figure 7: The thermal stress distribution of different rods in the same module. (a) Module 1. (b) Module 6. (c) Module 16.

shadow at 0~900 s. After the antenna has entered the shadow area completely, the temperature decreases rapidly. At 1800 s, the antenna structure begins to come out of the shadow area, the temperature of each chord changed contrary to the process of entering the shadow area. Finally, the antenna structure returns to its original temperature at 3600 s. The thermal analysis results are used as the basis for the thermal-structural analysis.

4. Thermal-Structural Analysis of the Antenna Structure

4.1. Model Overview. The ANASY finite-element analysis software is used to analyze the thermal-structural model of the modular support structure including the stress development and development-time history in the transient temperature field. The transient temperature field obtained in Section 3.2 is used as the temperature boundary conditions for the thermal-structural analysis of the antenna, and the temperature elements (LINK33) are converted into structural elements (LINK180). When the antenna is deployed in the orbit, one vertical rod is attached to the deployment boom of the satellite antenna. In Figure 4, the vertical rod BB' is used as the fulcrum of the expansion where the modular structure begins to unfold. Hence, its rotational angle and displacement in the x, y, and z directions are constrained. It is assumed that the thermal expansion coefficient of the structural elements does not change with the change in the temperature field, i.e., the stress and displacement of the antenna structure at 273.15 K are equivalent to 0. The thermophysical properties of the structural elements are listed in Table 1.

4.2. Thermal Stress Analysis. Indirect thermal stress analysis was carried out, and the obtained transient temperature field was applied to the structural stress analysis as the basic load. The maximum thermal stress variation of the components

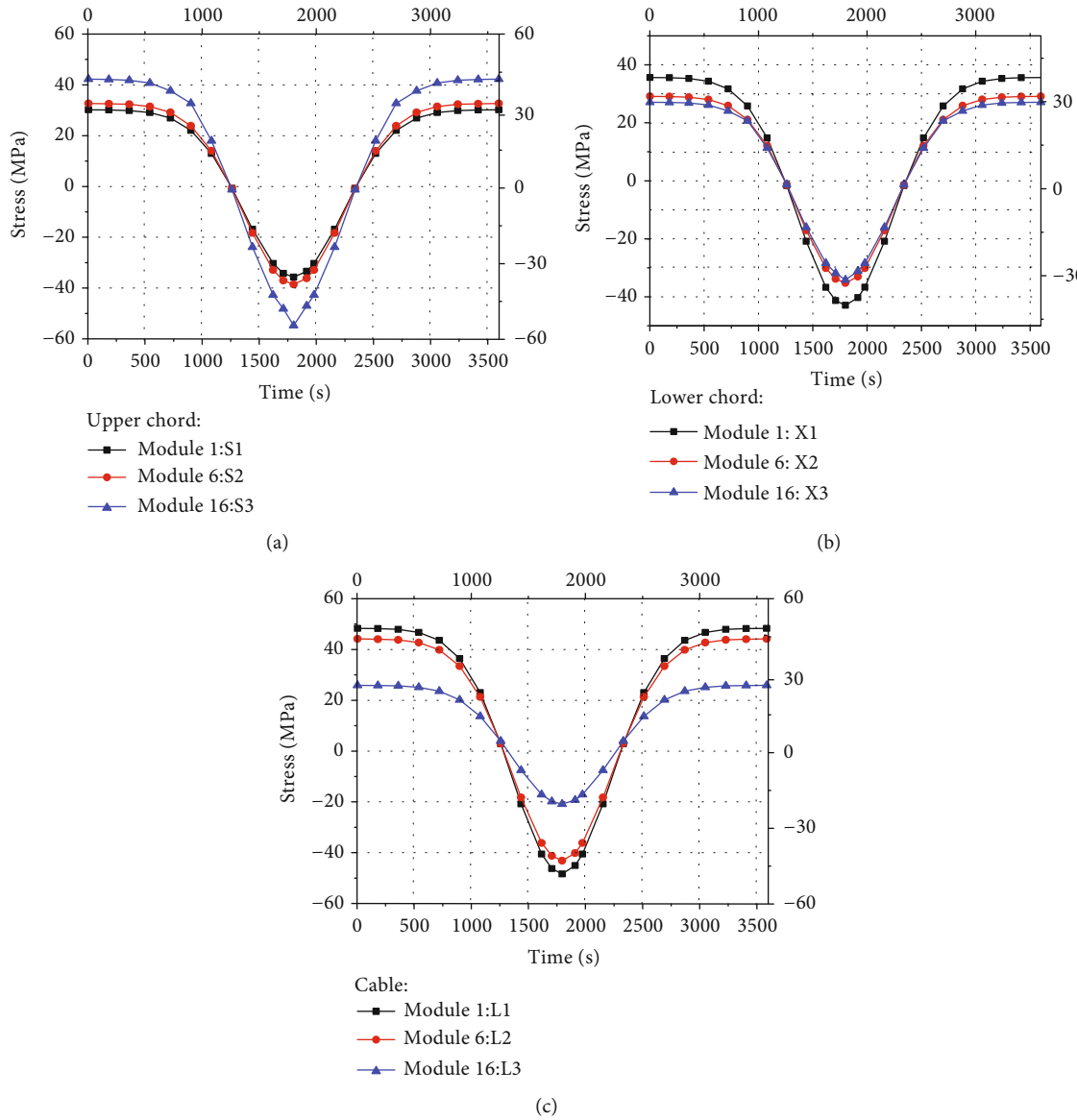

Figure 8: Thermal stress distribution of the rods in different modules. (a) Upper chord. (b) Lower chord. (c) Cable.

and the deformation trend of the centroid and edge of structure were obtained, and the statistics were shown in Table 2. It can be seen in Table 2 that the maximum normal stress of the chord at each time occurs at the 12th module and the minimum stress occurs at the vertical rod BB′. The maximum stress of the cable occurs at the first module of the structure. The maximum cumulative deformation of the antenna occurs at the point D4-X where it is the farthest point away from the constraint BB′, and the deformation is within the range of 32.05 mm~−39.02 mm. The deformation at the upper centroid point D1-S is within the range of 13.15 mm~−15.91 mm. So, it is gained that the effect of thermal deformation of the structural centroid on the antenna surface accuracy cannot be ignored.

The deformation and stress changes of the structure are consistent with the transient temperature field curve. At both 1 s and 3600 s moment, the maximum normal stress of the chord is 50.67 MPa and that of the cable is 47.94 MPa. In the meantime, the maximum deformation at D4-X is 32.05 mm. The deformation and stress of the antenna structure are very small at 1260 s and 2340 s, and the temperature is 293.15 K. At 1800 s, the maximum negative stress of the chord rod in the 12th module is −61.92 MPa and that of cable L1 in the central module is −58.84 MPa and the cold shrinkage deformation is −39.02 mm at this moment. However, compared to other rods, the thermal stress of the vertical rod at constraint BB′ is negligible. At each time, the maximum stress of the chord in the 12th module is about 5.23% greater than the average stress of the cable in the central module, indicating that the chord is subjected to greater stress than the cable in the transient temperature field.

Next, the transient temperature field at $t_1 = 900$ s and $t_2 = 1800$ s is used to analyze the thermally induced stress in different modules and the deformation of the antenna structure.

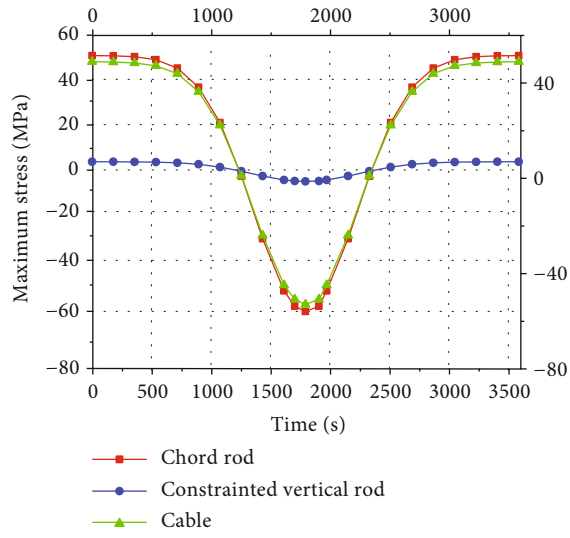

Figure 9: Time history of the maximum thermal stress.

Figure 6 shows the thermal stress distribution of each module of the antenna structure. It can be seen in Figure 6 that the stress distribution trend of the support structure is basically the same at each moment. In the central module, the cable stress is the largest, followed by the lower chord stress, and the upper chord stress is the least. In the second-circle module, the 6th module is taken as an example, the cable stress is the largest, followed by the upper chord stress, and the lower chord stress is the least. In the 16th module of the third circle, the stress of the upper chord is the largest, that of the lower chord is smaller, and the cable stress is the least. In addition, with the increase of circle, the stress of chord rod increases and the cable stress decreases gradually.

In order to further explain the stress development of structural component rods, the upper chord, lower chord, and cable stress of the 1st, 6th, and 16th modules were extracted and compared. Figure 7 shows the thermal stress distribution of the different component rods in the same module, and that of the same component in the different modules is shown in Figure 8.

In Figure 7, the thermal stress of upper chord S1 in the first module is 8.87% smaller than that of lower chord X1. In the 6th module that belongs to the second circle, the stress of upper chord S2 exceeds that of lower chord X2 by 17.3%. The cable thermal stress is the biggest in the 1st and 6th modules, the thermal stress of chord S1 is smaller than that of lower chord X1, and upper chord S2 in the 6th module is bigger than lower chord X2. In the 16th module, the thermal stress of cable L3 is the smallest and the maximum stress of upper chord S3 is bigger than that of L3 about 52.27%.

Figure 8 shows the comparison of the same component's thermal stress in the 1st, 6thm and 16th modules of the antenna structure, and the thermal stress of upper chord S1 decreases by 7.72% and 33.22% compared with that of upper chord S2 and S3, while the thermal stress of lower chord X1 increases by 22.43% and 24.97% compared with that of X2 and X3, respectively. The thermal stress of cable L3 is 46.58% and 51.42% lower than that of cable L2 and L1. Additionally, it was determined that the stress of the upper chord components increases gradually with each circle modules, whereas the stress of the cables gradually decreases.

The time history of the maximum thermal stress in the different components is shown in Figure 9. It is evident that the lowest of stress occurs in the constrained vertical rod at any moment. Moreover, the maximum stress trends for different components are consistent with the transient temperature field. Specifically, when the antenna structure begins to pass through the Earth's shadow at about $t_1 = 900$ s, its thermal stress decreases by approximately 27.45%. The maximum negative stress occurs at $t_2 = 1800$ s; at this moment, the antenna is passing through the Earth's shadow. After 1800 s, the thermal stress begins to increase again and mirrors the decreasing temperature trend before $t_2 = 1800$ s until the antenna has passed the shadow area completely.

The deformation curves of the key positions such as the vertical rod BB′, the centroid point D1-S(X), and the farthest point D4-S(X) from the constraint are shown in Figure 10. It can be seen that during the time from 0 s to 1260 s and 2360 s to 3600 s, the structure is in the thermal expansion and elongation stage, and in the middle period from 1260 s to 2360 s, the structure has cold contraction deformations. There is almost no deformation at the restraint vertical rod BB′. The deformation trend at the positions D4-S(X) and D1-S(X) is consistent with the time. The deformations of the upper and lower key points are not different significantly, and the accumulated deformation at D4-X is the largest. The deformation at the upper centroid point D1-S varies in the range 13.15 mm~−15.91 mm, where it is the most important factor affecting the accuracy of the antenna surface. Therefore, the influence of centroid point deformation on the accuracy of the antenna surface should be further studied.

The overall deformation of the structure at typical moment $t_1 = 900$ s and $t_2 = 1800$ s is shown in Figure 11. It is obvious that the further point away from the constraint, the greater the total cumulative deformation of the structure at this point and the maximum deformation of the antenna structure occurs at point D4-S(X) which is farthest from the constraint.

The aforementioned analysis shows that the antenna structure undergoes thermal expansion and contraction in the transient temperature field. In the first module, the stress in the upper chord and lower chord rods does not significantly change because of the action of the tension cables. However, in the second-circle and third-circle modules, the upper chord components expand and contract more than the lower chord because the cables inside the parabolic support structure undergo higher tension due to temperature variations in the transient temperature field. Consequently, the thermal stress in the upper chord components is higher. The highest thermal stress occurs in the third-circle modules. Therefore, the deformations of the farthest point from the constraint and the centroid point of structure cannot be ignored.

4.3. Thermal Analysis of Structures with Different Constraints. This section elucidates the effect of the

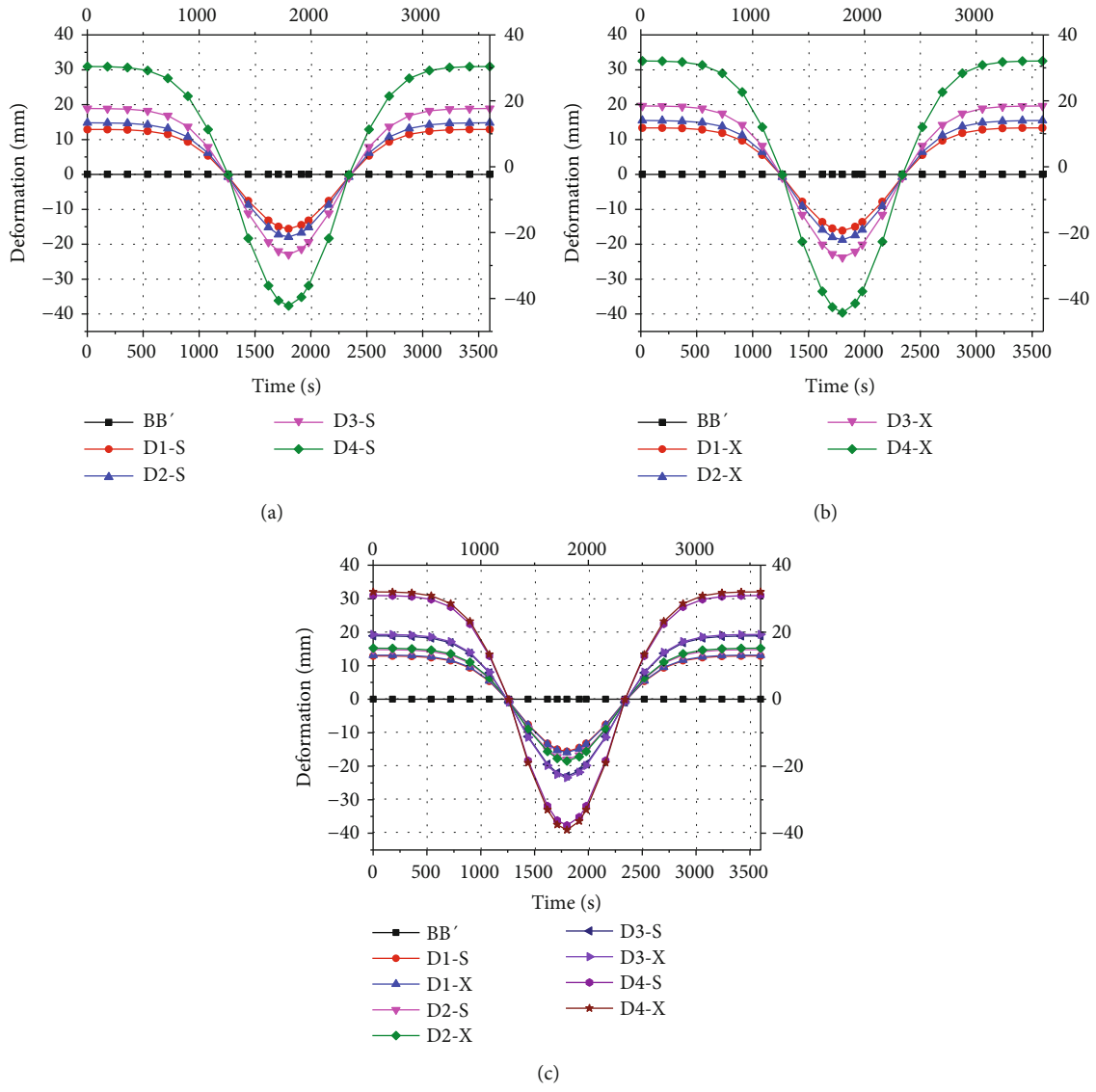

Figure 10: Time history deformation curve at key points of antenna structure. (a) The upper rods. (b) The lower rods. (c) The upper and lower rods.

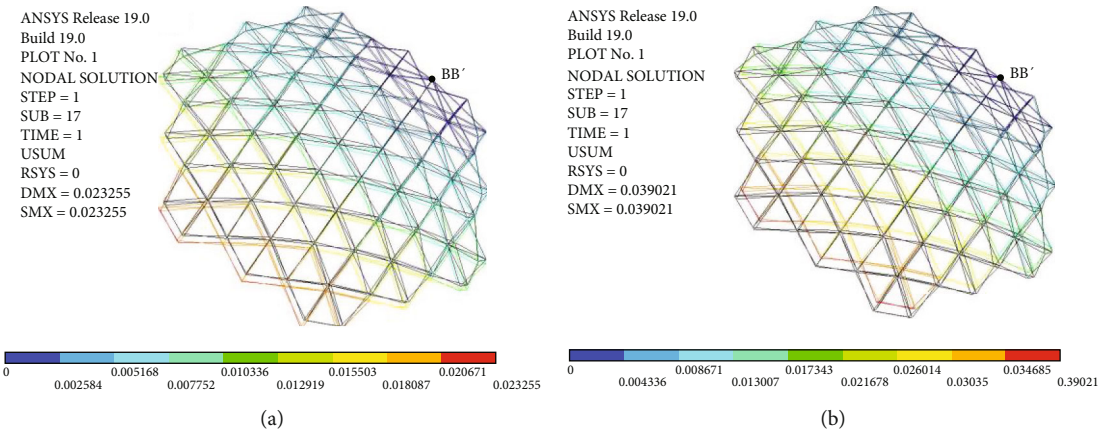

Figure 11: Overall deformation of the antenna structure. (a) $t_1 = 900$ s. (b) $t_2 = 1800$ s.

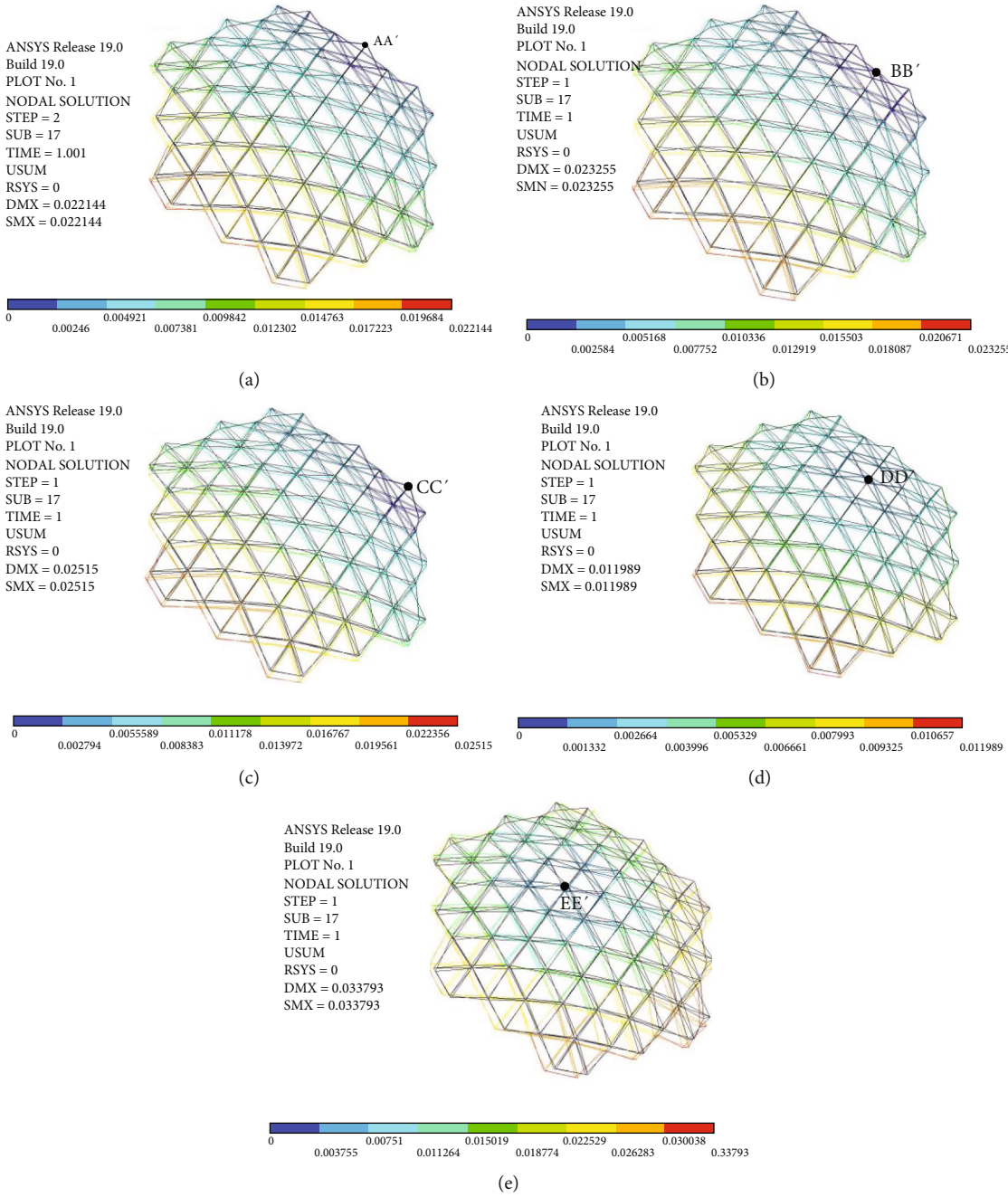

Figure 12: Overall deformation of structures with different constraints. (a) The constraint at AA′. (b) The constraint at BB′. (c) The constraint at CC′. (d) The constraint at DD′. (e) The constraint at EE′.

constraint position on the centroid D1-S(X) deformation of the antenna in the transient alternating temperature field. The vertical rods AA′, BB′, CC′, DD′, and EE′ of the structure are assumed to be the fulcrums of antenna expansion, separately. When the constraint is set at the abovementioned five vertical rods separately, the overall deformation of the antenna support structure at $t_1 = 900$ s is shown in Figure 12.

According to the application status of the antenna structure, the outermost vertical rod is the preferred position of the expansion fulcrum. When the constraint position of the antenna structure is required to be at AA′, BB′, and CC′ separately, the overall deformation of the structure constrained at the vertical rod CC′ is the largest and that of structure constrained at BB′ is slightly smaller and the structure constrained at AA′ deformation is minimum. Although the deformation in the case constrained at AA′ is smaller than that of the case at BB′ slightly and the vertical rod at BB′ has stronger stiffness because it is located at the splicing of two adjacent modules, so, the vertical rod BB′ is more conducive to being the fulcrum of antenna structure expansion, as shown in Figure 12(b).

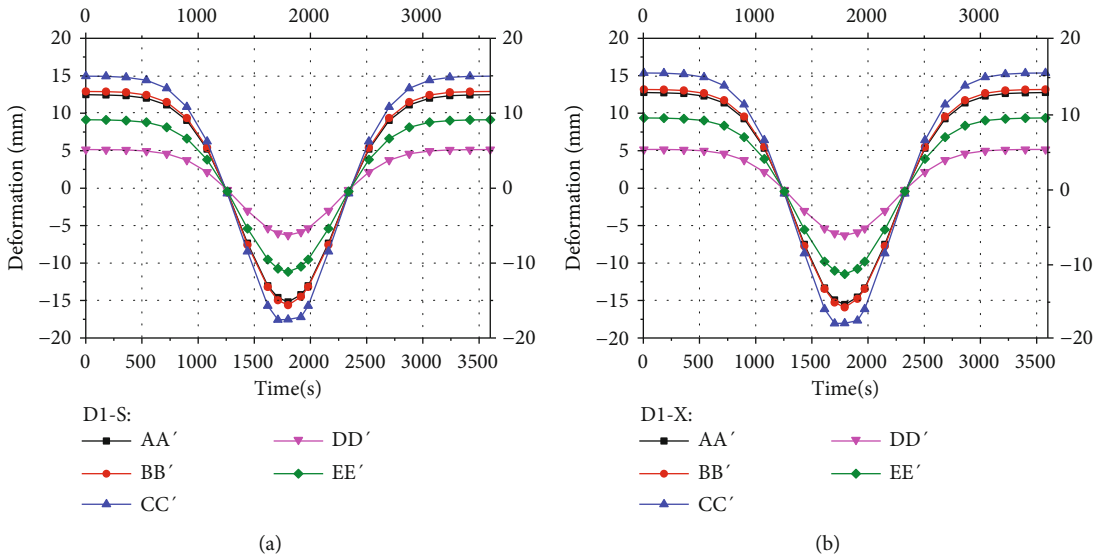

Figure 13: Thermal deformation curves of the centroid at different constraints. (a) Deformation of centroid D1-S. (b) Deformation of centroid D1-X.

If it is possible that the middle vertical rod, such as DD′ and EE′, inside the antenna is used to be the expansion fulcrum, the overall deformation of the structure constrained at DD′ is smaller than that at EE′. Moreover, because there is a large torsion ratio for the structure constrained at the EE′ vertical rod, so, it is better to choose the DD′ vertical rod as the middle expansion fulcrum of the antenna structure; see Figure 12(d).

The deformation development of the centroid D1-S(X) at different constraints with the temperature history is shown in Figure 13. Comparing between Figure 13(a) and Figure 13(b), the deformation trends of upper centroid D1-S and lower centroid D1-X are consistent with changes in temperature under working conditions at different constraints. The maximum difference of deformation between D1-S and D1-X is 3.33% under condition at constraint BB′, and the total average difference is 2.04%, indicating that there is little difference between D1-S and D1-X at each constraint.

The deformation amplitude of centroid D1-S of the upper layer structure constrained at AA′ is 12.47 mm~ −15.20 mm, and at any moment, the deformation is the smallest in the case of the edge constraint. Compared with the constraint at the CC′ vertical rod, its deformation is reduced by 17.42% and the total average deformation is reduced by 16.3%. Compared with the constraint BB′ case, the deformation decreases by about 3.44% and the average deformation decreases by about 3.02%. The D1-S deformation is within the range of 5.15 mm~−6.27 mm in the case constrained at DD′, and the deformation is the smallest under all working conditions. Compared with the constraint EE′ case, the maximum deformation of D1-S is reduced by 43.95% and the average reduction is about 43.66%. Compared with the constraint AA′ case, the deformation of D1-S is reduced by 56.71% and the total average reduction is 56.94%.

Based on the aforementioned results, when the expansion fulcrum of the antenna is set at the outermost vertical rod of the structure, it is suggested that the structure constraint should be applied at the splicing vertical rod of two outermost adjacent modules; the comprehensive performance of the structure is optimal in this case, such as BB′ as shown in Figure 2. When the fulcrum can also be located in the middle of the antenna, it is suggested that the constraint of the support structure should be selected at the splicing vertical rod of the adjacent modules in the second circle, such as DD′ in Figure 2. The constrained vertical rod serves as the connection between the antenna structure and the satellite boom. No matter where is the constraint, the range of thermal deformation due to the transient temperature field should be limited. It can reduce the adverse effect of thermal deformation on the surface accuracy of the modular deployable antenna.

5. Conclusions

In this study, the thermal analysis and thermal-structural analysis of the modular space-deployable antenna support structure under the action of the alternating temperature field are carried out and the thermal stress and deformation development law of each component in the antenna are obtained. The influence trend of the constraint position on the structure central and overall deformations is studied. Finally, the optimal constraint position of the antenna is suggested. The main conclusions of this study are as follows.

(1) During the thermal analysis of the antenna structure, the temperature of each component element is assumed as in accordance with the transient temperature field and the overall temperature changes slowly when the antenna enters and exits the Earth's shadow area. Furthermore, the temperature drops significantly in the shadow area completely

(2) The transient temperature field obtained via structural thermal analysis can provide boundary conditions for the thermal-structural analysis. The thermal stress and deformation time history of the antenna structure are essentially consistent with the trend of the transient temperature field

(3) In same circle module, the thermal stress in upper chord rods is higher than that in lower chord rods and it progressively increases toward the outer edge of the antenna structure. When the thermal exchange amplitude of the deployable antenna structure is large, the accumulated deformation at the centroid of the upper structure can reach up to 15 mm and the influence on the mesh accuracy of the antenna structure cannot be ignored

(4) It is recommended to select the splicing vertical rod of adjacent modules in the outermost or the second circle as the constraint position of the antenna structure. The constrained vertical rod connects the antenna to the satellite boom, where it is also the expansion fulcrum of the antenna, and both the overall and central deformations of the structure will be limited to the allowable values in any case

(5) It is suggested that the thermal protection measures such as ZS-1 high-temperature-resistant thermal insulation coating should be adopted on the surface of the antenna support structure to increase the adaptability of the antenna in the extreme space environment. Using the abovementioned measures, the adverse influence of temperature alternation on the antenna deformation and the mesh surface accuracy can be reduced

This study presented preliminary work on thermal-structural analysis of the support structure for the modular space-deployable antenna under a uniform temperature field, and more complicated models considering rigid-flexible coupling and shadow occlusion could be used in the future to achieve more conclusions.

Data Availability

All data generated or analyzed during this study are included within the article.

Conflicts of Interest

The authors declare that there is no conflict of interest regarding the publication of this paper.

Acknowledgments

This research was supported by the key program of the National Natural Science Foundation of China (Grant no. 51835002), the China Postdoctoral Science Foundation (Grant no. 2019M661126), and the Foundation of Liaoning Education Department (Grant no. LJKZ0563). These supports are gratefully acknowledged by the authors.

References

[1] F. Hu, Y. Song, Z. Huang, L. Yichen, M. Xiaofei, and L. Wan, "Design optimization of modular configuration for deployable truss antenna reflector," *China Space Science and Technology*, vol. 42, no. 1, pp. 1–8, 2021.

[2] D. Tian, H. Gao, L. Jin et al., "Research status and prospect of modular space deployable and foldable mechanism," *China Space Science and Technology*, vol. 41, no. 4, pp. 16–31, 2021.

[3] Y. Ding, W. Shen, J. Li, Z. Cheng, J. Jin, and J. Sun, "Research on Trusted Full-Proxy Homomorphic Transmission Mechanism for Satellite Communication," *Chinese Space Science and Technology*, vol. 40, no. 4, p. 84, 2020.

[4] H. L. Qian, J. Zhong, and F. Fan, "Analysis on non-uniform temperature field due to sunshine for the antenna structure of Shanghai 65-meter-aperture radio telescope," *China Civil Engineering Journal*, vol. 43, no. 3, pp. 39–46, 2014.

[5] J. Wu, Z. H. Zhao, and G. X. Ren, "Dynamic analysis of space structure deployment with transient thermal load," *Advanced Materials Research*, vol. 1673, pp. 803–807, 2012.

[6] X. F. Ma, Y. Li, and Y. Xiao, "Development and tendency of large space deployable antenna reflector," *Space Electronic Technology*, vol. 15, no. 2, pp. 16–26, 2018.

[7] Z. Shen, Q. Tian, X. Liu, and G. Hu, "Thermally induced vibrations of flexible beams using absolute nodal coordinate formulation," *Aerospace Science and Technology*, vol. 29, no. 1, 2013.

[8] L. J. Cheng and D. M. Xue, "Thermal-dynamic analysis of large scale space structures by FEM," *Journal of Tsinghua University (Science and Technology)*, vol. 21, no. 5, 2004.

[9] Z. H. Chen, *Research on Synthesis of Shaped Reflector and Thermal Analysis of Antenna In-Orbit*, Zhejiang University, 2009.

[10] B. A. Boley, "Approximate analyses of thermally induced vibrations of beams and plates," *Journal of Applied Mechanics*, vol. 39, no. 1, pp. 212–216, 1972.

[11] E. A. Thornton and Y. A. Kim, "Thermally induced bending vibrations of a flexible rolled-up solar array," *Journal of Spacecraft and Rockets*, vol. 30, no. 4, pp. 438–448, 1993.

[12] R. Namburu and K. Tamma, "Thermally-induced structural dynamic response of flexural configurations influenced by linear/non-linear thermal effects," in *32nd Structures, Structural Dynamics, and Materials Conference*, U.S.A., 1991.

[13] J. D. Johnston and E. A. Thornton, "Thermally induced attitude dynamics of a spacecraft with a flexible appendage," *Journal of Guidance Control and Dynamics*, vol. 21, no. 4, pp. 581–587, 1998.

[14] S. J. Zhang, *Design and Thermal Analysis of Spatial Deployable Truss Structures*, Zhejiang University, 2001.

[15] Y. Ding and D. M. Xue, "Finite element analysis of transient temperature field and thermal deformation of space thin-walled circular tube under radiation heat transfer," *Journal of Astronautics*, vol. 23, no. 5, pp. 49–56, 2002.

[16] J. I. Rodriguez, A. Na-Nakornpanom, and J. G. Rivera, "On-orbit thermal performance of the TES instrument-three years in space," *SAE International Journal of Aerospace*, vol. 1, no. 1, pp. 364–375, 2009.

[17] L. J. Fan, J. Duan, Z. H. Xiang, D. M. Xue, and Z. Z. Cen, "Nonlinear finite element analysis of thermal-dynamics coupling system of large flexible spatial structures," *Journal of Astronautics*, vol. 30, no. 1, pp. 299–304, 2009.

[18] J. Liu, M. B. Zhu, and G. Cao, "Numerical analysis of thermal vibration of space borne deployable antenna," *China Space Science and Technology*, vol. 31, no. 2, pp. 53–57, 2011.

[19] L. K. Abbas, X. Rui, and P. Marzocca, "Aerothermoelastic analysis of panel flutter based on the absolute nodal coordinate formulation," *Multibody System Dyna-mics*, vol. 33, no. 2, pp. 163–178, 2015.

[20] Y. T. Sun, "Structure design and analysis of a space-borne antenna," *Electro-Mechanical Engineering*, vol. 34, no. 3, pp. 31–34, 2018.

[21] H. L. Yun and P. F. Yuan, "Thermal-structural analysis of hoop deployable antenna in real orbital environment," *Mechanical Science and Technology for Aerospace Engineering*, vol. 38, no. 10, pp. 1612–1618, 2019.

[22] C. K. Wu, B. Y. He, and P. F. Yuan, "Thermal-structural analysis of hoop deployable antenna with metal hinges," *Chinese Journal of Engineering Design*, vol. 27, no. 3, pp. 349–356, 2020.

[23] S. Corpino, M. Caldera, F. Nichele, M. Masoero, and N. Viola, "Thermal design and analysis of a nanosatellite in low earth orbit," *ActaAstronautica*, vol. 115, pp. 247–261, 2015.

[24] P. Yeonkyu, K. Geuknam, and P. Sangyoung, "Novel structure and thermal design and analysis for cubesats in formation flying," *Aerospace*, vol. 8, no. 6, p. 150, 2021.

[25] R. Q. Liu, D. K. Tian, Z. Q. Deng, and H. W. Guo, "Modal analysis of truss structure for deployable truss antenna with multi module," *Transactions of Beijing Institute of Technology*, vol. 31, no. 6, pp. 685–690, 2011.

[26] D. K. Tian, *Design and Experimental Research on Truss Structure for Modular Space Deployable Antenna*, Harbin Institute of Technology Press, 2012.

[27] X. An and G. Feng, "Thermally induced vibration of the main mast of the space station's solar arrays," *Structure and Environment Engineering*, vol. 32, no. 3, 2005.

[28] G. G. Yang, M. B. Zhu, P. Y. Lian, F. Gao, and Y. L. Zong, "Thermal induced coupling-dynamic analysis of a deployable satellite antenna system," *Journal of Vibration and Shock*, vol. 33, no. 24, pp. 173–178, 2014.